City, University of London Institutional Repository

This is the accepted version of the paper.

This version of the publication may differ from the final published version.

Permanent repository link: https://openaccess.city.ac.uk/id/eprint/23504/

Link to published version: https://doi.org/10.1109/tbcas.2019.2959437

Modelling Dynamically Re-sizeable Electrodes (DRE) for Targeted Transcutaneous Measurements in Impedance Plethysmography

Zaheer Q. Hashim, *Member, IEEE*, Loukas Constantinou, *Member, IEEE*, and Iasonas F. Triantis, *Member, IEEE*

Abstract—Impedance plethysmography of extremities typically uses band electrodes around limbs to monitor changes in blood volume. This often causes monitored blood variations to only generate minuscule impedance values relative to the measured baseline, attributed to the tissue surrounding the artery or vein of interest. Smaller, ECG type electrodes can provide a larger signal, however their output is very easily affected by the placement of the electrodes relative to the targeted vasculature. This paper presents a novel method to adjust the active surface of electrodes, introducing Dynamically Re-sizeable Electrodes (DRE), to only target the exact area of interest, forming localised electrodes, without having to manually re-position them. Elongated rectangular electrodes were partitioned into smaller electrode segments, interconnected through custom circuitry. For the development and assessment of the DRE system, work was carried out both experimentally in-vitro on gelatine phantoms using custom switching circuits and through finite element modelling (FEM) simulations in COMSOL. A scanning sequence made use of DRE in single segment variable tetra-pole (SSVT) mode proved capable to identify the transcutaneous location of the blood vessel of interest and the specific electrode segments located in its vicinity. Impedance measurements were then taken using these segments connected to form localised electrodes only placed over the targeted vessel. The resulting localised electrodes exhibited up to 28% increased sensitivity to blood variations relative to larger electrodes.

Index Terms—Impedance plethysmography, segmented electrodes, impedance, localised measurements

I. INTRODUCTION

IMPEDANCE plethysmography (IPG) is a simple non-invasive method that can be used for monitoring changes in blood volume in the limbs or in the thorax [1] to assess, amongst other metrics, cardiac parameters such as cardiac output and stroke volume [2]. Unlike other photo-plethysmography (PPG), IPG uses electrical currents in order to take measurements instead of light, therefore it is not influenced by ambient light or skin pigmentation. IPG can also be used to get signals from a large number of sites [3]. Through the placement of four electrodes (tetrapolar method [4]) on the skin, impedance (or bioimpedance) measurements are taken by injecting a low amplitude alternating current and measuring the resulting potential developed across the tissue beneath the electrodes [5].

Z. Hashim, L. Constantinou and I.F. Triantis are with the Department of Electrical and Electrical Engineering, City, University of London, London, United Kingdom, e-mails: [zaheer.hashim, loukas.constantinou, i.triantis] @city.ac.uk

The method has been demonstrated with band electrodes wrapped around the neck and the abdomen for cardiac output measurements across the thorax [6], or around a limb (Fig. 1(a)) [2], [7], [8], e.g. for monitoring blood volume variations in the brachial artery [9], [10]. Band electrodes have, however, a major drawback: in addition to the impedance of the tissue of interest – in this case blood – measurements also include the impedance of the surrounding tissue. Given the low impedance value of blood relative to all other tissue types, this leads to a significant yet undesirable measurement baseline that overshadows the small magnitude changes caused by blood volume variations [11]. In order to address this, the use of smaller electrodes (e.g. ECG electrodes) has been proposed [1], [6], [11], [12], close to the vascular structure of interest.

Experimental comparisons have shown that such electrodes provide a larger signal to noise (redundancy) ratio compared to band electrodes [11] in addition to other benefits including causing less discomfort to the patients [6] and potentially removing the effects in the measurement of surrounding vessels. Such measurements are, however, very sensitive to the placement of the electrodes [2], [12] relative to the targeted vasculature. This issue is not easy to address practically both because that target may be difficult to locate and also because once located the electrodes would have to be re-positioned until aligned, causing discomfort and potentially destroying their adhesion. It is therefore desirable to develop impedance measurement electrodes whose active surface can be adjusted to target only the exact area of interest, forming localised electrodes, without manually re-positioning them.

In this paper a novel approach to targeted impedance plethysmography measurements with dynamically re-sizeable electrodes (DRE) is presented. A system involving electrodes of adjustable effective size has been developed. Four elongated rectangular electrodes [8] (named hereafter stripe electrodes as in Fig. 1(b)) have been partitioned into smaller electrode segments (Fig. 1(c)) which are interconnected through custom circuitry. This allows any of the segments of each of the four partitioned electrodes to be individually addressed to form single-segment variable tetrapoles (SSVT, Fig. 2c); or to be grouped so as to just cover the targeted vasculature, thus forming effective localised electrodes to provide more targeted measurements. When all segments of each of the four partitioned electrodes are shorted they each form an effective stripe or a pseudo-stripe electrode. The developed prototype DRE system was simulated using finite element modelling (FEM) analysis (COMSOL v.5.3a) and experimen-
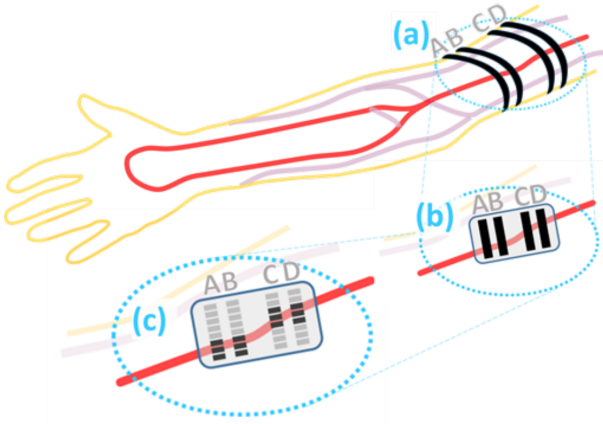
Fig. 1: Simplied diagram showing positioning of electrodes using: a) Band electrodes taking measurements from the whole section of the arm, b) Stripe electrodes taking measurements over the vessel and the surrounding tissue and c) Segmented electrodes grouped into localised effective electrodes to take measurements only over the targeted vessel.

tally verified in-vitro by performing impedance measurements, through custom-made instrumentation, using gelatine phantoms to mimic tissue characteristics.

Section II deals with the lumped impedance and geometric model parameters, the electrode and circuit design, the in-vitro experimental and simulation setup. Section III presents the experimental and the simulation results obtained. From the conclusions summarised in Section IV it follows that the new DRE allows measurement localisation and improves the signal to noise ratio in impedance plethysmography for targeted vascular structures accessed transcutaneously.

II. METHODS

An approximate biological model of a subcutaneous blood vessel was constructed and simulated. It was idealised so as to assess the DRE method and thus only a single frequency was considered, bone and muscle were not included and the model dimensions were limited to allow for the surface of the skin to be approximated as flat rather than curved. Moreover the model considered only one vessel in the examined volume. The features considered, although geometrically idealised, were kept consistent with anatomy. The vessel was modelled in various orientations (θ) relative to the electrode tetrapole. Two research questions where assessed: 1) whether through SSVT the blood vessel location could be determined; and 2) whether the resulting localised electrodes are more sensitive to variations in the blood vessel properties relative to the larger stripe electrodes.

A. Geometric Model Parameters

A parallelepiped geometric model with length, width and height of 45 mm, 20 mm and 10 mm respectively was designed to examine the aforementioned two research question (Fig 2a). The model was used as a template for both the gelatine phantom used in experiments and for the FEM simulations.

(a) 3D Model

(b) Stripe electrode dimensions

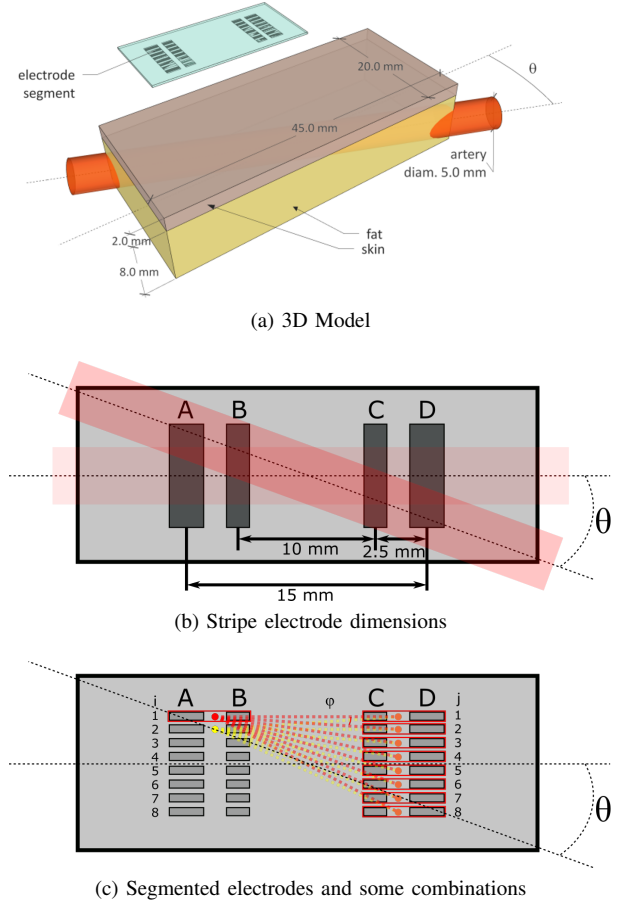(c) Segmented electrodes and some combinations

Fig. 2: Overall dimensions for top view of simulation model for both electrode setups. a) a 3D representation of the model geometry, b) Stripe electrode setup with dimensions (top view). c) Segmented electrode setup with some segment combinations shown (top view)

It was based on the brachial artery of the arm, which has been used with IPG [13]], with a worst-case scenario configuration whereby the artery is surrounded by fat, which is significantly less conductive than blood. It featured three main structures of homogeneously conductive geometries: a $2\ mm$ thick skin layer, a $8\ mm$ thick fat layer and a $5\ mm$ diameter cylindrical blood vessel embedded in the latter. The blood vessel's longitudinal axis was on a plane parallel to- and $7\ mm$ deep from the skin surface plane on which the electrodes were attached. Assuming that, realistically, perfectly in-line placement of the electrode tetrapole relative to the blood vessel would be very difficult to achieve, tests - mainly in simulations as described later - were designed to mimic imperfect placement by involving a number of orientations (θ) of the vessel relative to the tetrapole's middle axis of symmetry (i.e. the axis connecting the electrodes across their centres).

B. Tissue properties

The electrical properties of biological tissue are frequency dependent and have conductive and reactive elements [14] and

impedance plethysmography measurements have been mostly reported at frequencies between 10KHz − 100KHz [15], [4]. In simulation, it is fairly easy to assign conductivity and relative permittivity of different types of tissue to sections of the 3D model used for simulations [16]. However, when modelling biological tissues experimentally using gelatine phantoms, it is not straightforward to replicate the reactive element [17], [18], [19], and thus the conductivity of tissue that corresponds to the impedance magnitude at a particular frequency of choice is mostly used . For the simulation model used here the conductivity values for skin, fat and blood were set to 2.937mS/m, 42.954mS/m and 700.04mS/m and the relative permittivity values were set to 29010, 911.54 and 5248.2 respectively corresponding to impedance measurements at a frequency of 10KHz as reported in [20], [21]. For the experimental phantom, the conductivity values can be altered by varying the concentration of NaCl (sodium chloride) in the solution used to create the phantom [18]. That frequency value was at the lowest end of the aforementioned spectrum and it was selected to represent a worst case scenario in terms of skin and fat layers impeding the injected current.

C. Electrode Design

Impedance values were to be extracted through electrodes attached to the skin layer surface in both the experiments and the simulations. For current injection electrodes it is important to have a relatively large area to reduce the electrode-electrolyte interface impedance so as to avoid overloading the current injection circuitry. The voltage measurement electrodes can be made smaller − as their interface impedance can be ignored − increasing the measurement precision and the signal-to-noise ratio of measured data [22]. Therefore here four stripe electrode sites A, B, C and D were considered (fig 2b), with the current injection electrodes A and D having a $2\ mm\ \times\ 8\ mm$ geometry, and the voltage measuring electrodes B and C being $1.5\ mm\ \times\ 8\ mm$. The length of the electrodes was chosen so as to adhere to the dimension limitations of the model - so as to approximate the arm skin as being flat - and it closely resembled electrodes used in [23]. Each stripe was subdivided into eight $0.6\ mm$ long segments separated by a $0.4\ mm$ gap (fig 2c). The centre to centre distances were $15\ mm$ for electrodes A and D and $10\ mm$ for B and C, resulting to a $2.5\ mm$ distance between each of electrodes A-B and C-D. The electrode spacing was designed cover adequate length of the blood vessel so as to increase the volume of the blood contributing to the measurements.

D. Lumped-impedance simplified representation

In order to ascertain the theoretical basis of research question 2, prior to the experimental and the simulation assessments, an approximate analysis can be offered through a lumped impedance representation of the cases involving localised versus longer electrodes. It has generally been shown that the impedance of different tissue layers can be approximately represented by simplified lumped impedance models [24], [25], [26]with impedance magnitudes at the applied frequency considered. Following the geometric model presented

(a) Simplified lumped impedance side view
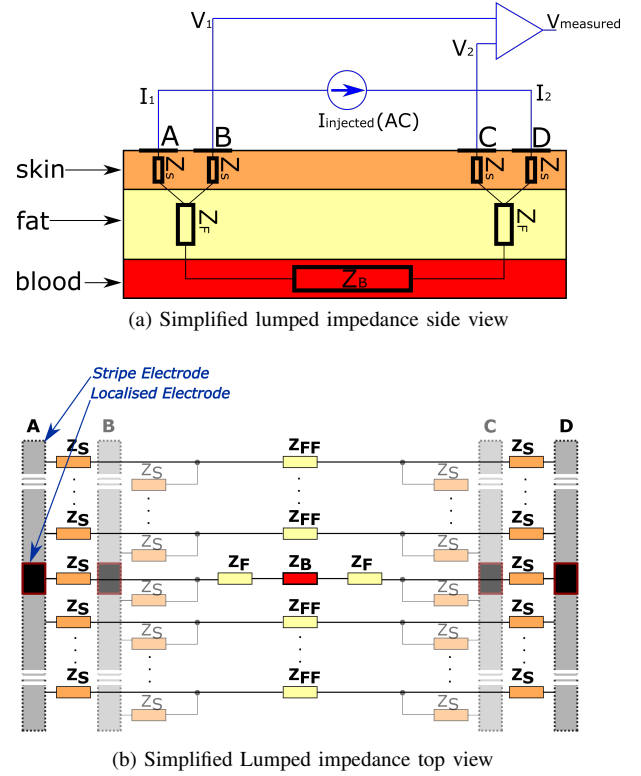

(b) Simplified Lumped impedance top view

Fig. 3: Simplified lumped impedance model. a) shows the simplified lumped impedance from the side, b) shows the simplified lumped impedance looking through the electrodes (top view)

previously, and assuming $\theta = 0$, Fig. 3 illustrates schematically a simplified lumped impedance model for a cross section of juxtaposed skin, fat and blood layers, with respective impedance magnitudes Z_S, Z_F and Z_B, respectively. A side view is shown in Fig. 3a, while Fig. 3b is the top view (from the skin down to the fat layer) of current paths along the tetrapole, assuming the blood vessel is on the axis connecting the electrodes across their centres.

The nature of electric/ionic current is to travel between two electrodes by taking the path of least resistance, and with the skin being the most insulating layer, currents will mostly traverse it flowing through it to the more conductive layers below [27]. Currents originating directly above the vessel will cross the skin and fat layers almost vertically and will enter the blood, flowing across it for a length approximately equal to the distance A-D. Currents flowing between electrodes A-D outside of the boundaries - but in the vicinity of the blood vessel will deviate from their straight geometric path and pass through it. As the length of the injecting electrodes extends away from the centrally located vessel currents adequately far from it will experience a minimum resistance path by traversing the skin and traversing fat tissue of equal length to the distance travelled inside the vessel by the centrally located field lines. The corresponding fat impedance magnitude in that case is shown as Z_{FF}. For a specific value of Z_B, the baseline impedance value $Z_{LOCbase}$ if localised electrodes are used, and the minimum corresponding baseline impedance

value $Z_{STRbase}$ when longer stripe electrodes are used, are calculated below. The stripe electrodes used in this calculation are long enough so as to allow n current paths to pass through fat surrounding the blood vessel.

Localised electrodes baseline impedance:

$$Z_{LOCbase} = 2Z_S + 2Z_F + Z_B \tag{1}$$

Larger stripe electrodes baseline impedance (n paths not passing through the vessel):

$$Z_{STRbase} = \frac{1}{\left(\frac{1}{Z_{LOCbase}} + \frac{n}{2Z_S+Z_{FF}}\right)} \tag{2}$$

because $Z_{STRbase}$ is the parallel combination of $Z_{LOCbase}$ and n parallel branches of $2Z_S+Z_{FF}$.

In order to examine which electrode type is more sensitive to blood variations, Z_B is assumed to change by x, with pulse related blood impedance variations typically amounting up to $\pm 20\%$ of the baseline value [4], [28]. The resulting variations to the overall impedance between A-D using localised vs larger stripe electrodes are calculated below. Localised electrodes impedance, using $2Z_S + 2Z_F = \alpha$, for clarity:

$$Z_{LOC} = \alpha + Z_B(1 + x) \tag{3}$$

Stripe electrodes impedance, using $2Z_S + Z_{FF} = \beta$ for clarity:

$$Z_{STR} = \frac{1}{\left(\frac{1}{Z_{LOC}} + \frac{n}{\beta}\right)} \tag{4}$$

Each configuration's sensitivity can be derived by the respective partial derivatives with respect to x [29], which respectively result to:

$$\frac{\partial Z_{LOC}}{\partial x} = Z_B \tag{5}$$

$$and \qquad \frac{\partial Z_{STR}}{\partial x} = \frac{Z_B\beta^2}{(n(1+x)Z_B + \beta + n\alpha)^2} \tag{6}$$

The ratio RLS of localised to stripe sensitivities yields:

$$and \qquad RLS = \frac{(nZ_B(1+x) + \beta + n\alpha)^2}{\beta^2} \tag{7}$$

As none of α, β, n and Z_B are negative (being impedance magnitudes) and although realistically $|x| \leq 20\%$, it is evident that RLS is greater than unity even for an extreme - theoretical - range of $|x| \leq 100\%$ which would result to Z_B varying from 0 to double its baseline value. That indicates that localised electrodes will always exhibit higher sensitivity to blood impedance variations relative to their larger counterparts and thus research question 2 is theoretically justified by the above model.

E. Experimental Setup

1) Circuit Design: The DRE system was designed to function according to the block diagram shown in figure 4a. A printed circuit board (PCB) was designed featuring the four segmented electrode sites, as illustrated in Fig. 2. The board was fitted with a 3D printed rectangular wall attached around the electrodes using epoxy glue, allowing the use of liquids on the electrodes without shorting any circuitry. The electrode addressing electronics were positioned on the bottom layer of the same PCB, in order to reduce the distance between the electrodes and the addressing circuitry. This served to minimise the influence of parasitics and noise in the impedance measurements and to further protect the latter from any accidental spillage of liquids. The addressing circuitry was developed for interconnecting and individually addressing the 32 segments of the DRE system and for interfacing the ones selected from each group A, B, C or D with the respective four channels of a tetrapolar impedance analyser (Keysight E4980A/AL Precision LCR Meter [30]). The requirements on the circuit, for real diagnostic use rather than for the static gelatine phantom scenario examined here, included minimal impedance contribution when active, fast switching and stable frequency response at the chosen carrier frequency. Fig. 4a shows the block diagram of the system which was implemented through the circuit diagram shown in Fig. 4b. Switching between segments was carried out using four ADG714 eight-analogue-switch ICs, featuring low on resistance (Ron = 2.5 Ω) and requiring about 28ns each to go from OFF state to ON and then OFF again. The ADG714 ICs were labelled 'U1' to 'U4'. To change the segment allocation, an 8 bit binary word needs to be sent serially to the ADG714 IC, each bit of the byte corresponding to one switch in the IC. In order to send the byte of switching data, the address pin of the desired IC needs to be held low and then high again to implement the switching data. The ADG714 ICs were controlled by a PIC18F26K22 micro-controller, with the switching data transmitted through the serial peripheral interface (SPI) pins, allowing them to connect each of the electrode segments individually or in combinations to the respective LCR meter channels (I_1, V_1, V_2, I_2). The user could select the segment combinations through switches activating pre-programmed sequences in the micro-controller. The pre-programmed sequence is then triggered using push-buttons. Three main sequences were pre-programmed into the micro-controller; the first sequence shorted all the segments to form the pseudo-stripe electrodes, the second sequence was the SSVT scanning sequence and the third sequence was the localised electrode sequence.

2) Gelatine Phantom Design: The experimental setup featured gelatine phantoms constructed in accordance to the previously described biological model, with the aforementioned dimensions, featuring skin and fat layers, each with a cylinder representing a blood vessel embedded in the fat layer (fig 5). The phantoms were created using 3D printed moulds in which gelatine solutions with conductivities corresponding to each respective layer were poured successively. The skin side of the phantoms was attached to the electrode PCB. To
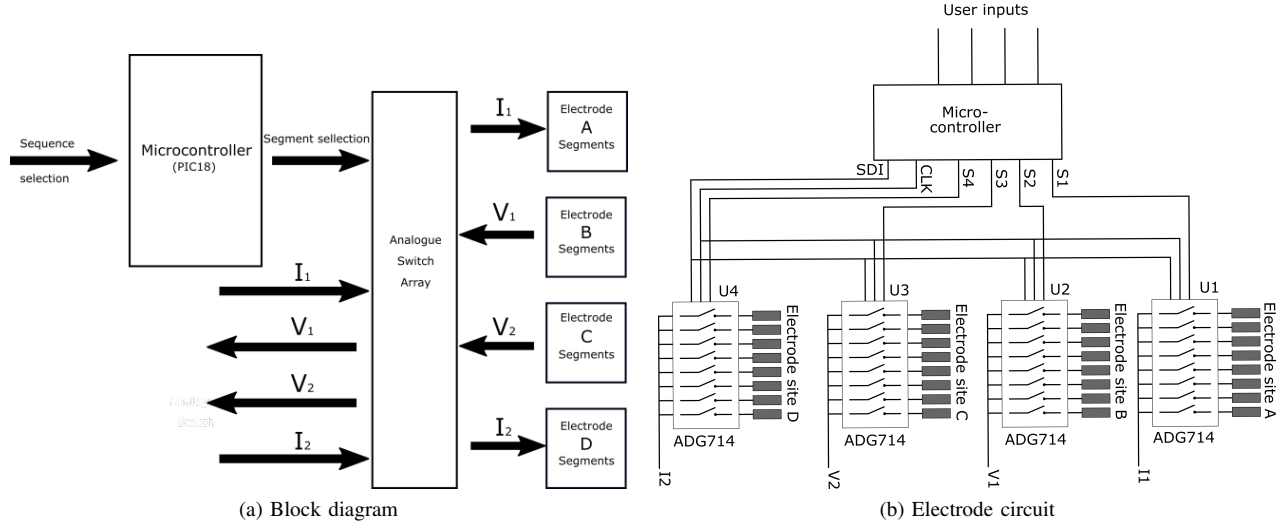
(a) Block diagram

(b) Electrode circuit

Fig. 4: Circuit diagram, a) shows the block diagram for the complete system. b) shows the connections to and from the micro-controller and the switch connection for the electrode segments sites to their corresponding impedance measurement channel

Fig. 5: Gelatine phantom comprising skin (yellow), fat (white) and blood vessel (red)

address research question (1), two phantoms P1 and P2 were constructed with their respective blood vessel cylinders placed at orientations of $20°$ and $-20°$ relative to the axis passing across A-D through the array's centre (fig. 2b). These values represented the maximum angles that allowed for the vessel to still be fully within the boundaries of the electrode area. To assess research question (2), five phantoms P2a-e, (variants of P2) were made with blood conductivity values between $700.04 mS/m$ (P2a $\equiv$ P2) and $1400.08 mS/m$, in steps of 25%.

3) Experimental Procedure: SSVT Sequence and Localised Measurements: For research question (1) and for each of the phantoms P1 and P2 described above, an impedance measuring sequence using DRE in SSVT mode was first carried out in order to find out which electrode segments were closest to the blood vessel. In each measuring sequence the injecting electrode segment from group A was always combined with the neighbouring measurement electrode segment from B, while the same combination was always observed between segments in C and D (Fig. 2c). The eight segments at each electrode site were designated by the electrode site followed by segment number (eg: A_1). Thus for each SSVT measurement a pair A_iB_i and a pair C_jD_j were used, with i,j independently having values between 1 and 8. An example of this is shown in figure 2c where segment pair A_1B_1 and its combination with all the C_jD_j segment pairs is shown with dashed-red lines.

A sinusoidal 10kHz, $100\mu A$ current was injected between A_i and D_j with B_i and C_j measuring the resulting voltage. The magnitude of the voltage between B_i and C_j was divided by the injected current magnitude to give the value of $|Z_{ij}|$ between the electrodes B_i and C_j. Each of the 8 A_iB_i pairs was combined in turn with each of the 8 C_jD_j pairs (dotted lines in Fig. 2c). The outcome of the sequence was thus an 8×8 matrix of 64 $|Z_{ij}|$ values.

When a scan is preformed using SSVT, the length of the active tetrapole varies. Even in a homogeneous volume this variation is the main factor that introduces non uniformity between the impedance values measured by each tetrapole [5], with other factors including boundary conditions and the fact that in this case the recording electrodes are not always in line with the current injection ones. In order to remove that scaling effect, each impedance value obtained from a SSVT tetrapole was divided by the length of that tetrapole. This approximate process significantly reduced the non-uniformity from the results. Subsequently, the values in the $|Z_{ij}|$ matrix were normalised between 0 and 100% and values lower than 10% of the resulting impedance range of the matrix were used to identify the electrodes closer to the vessel.

For research question (2) impedance measurements were then performed to the five phantoms P2a-e, first activating only the electrode segments from each group corresponding to lowest $|Z_{ij}|$ values, grouped to form the largest possible localised electrode covering only the area of interest. Each measurement was repeated with pseudo-stripe electrodes. Between each measurement sequence the electrodes were cleaned using ethanol to maintain good contact across the experiments and to remove any residue leftover from the previous experiments.

Pseudo-stripe electrode (i.e. using all A_iB_i and C_jD_j electrode segments) measurements were also carried out on saline solution, poured inside the 3D printed wall over the electrodes so as to occupy the same overall volume with the

gelatine phantoms. The conductivity of the saline used was 1.55 S/m as measured using Model 3540 pH/conductivity meter. These measurements were carried out for comparison with FEM simulations also featuring a saline.

F. FEM Simulations

Manufacturing phantoms controlling the electrical properties and accurately changing the orientation of the blood vessel was an elaborate time-consuming process. Implementing the different orientations in simulations would be quicker and would allow a more precise control over different parameters. Finite Element Modelling (FEM) simulations using the COMSOL 5.3 electric currents (ec) module under the AC/DC physics were first performed using SSVT on a saline parallelepiped model (conductivity of 1.55 S/m as measured previously), with identical dimensions to the geometric model and the phantom. In the ec module, quasi-static solutions of Maxwells equations were used to solve for the electrical potential. No electrode-electrolyte interface was included in the model. Electrode site A was assigned as a current terminal with a $1A$ current being assigned as a boundary condition. Electrode site D was assigned as a ground terminal of zero potential. It was assumed that no current flows through the exterior boundaries of the phantom, as the exterior boundary was air which is a poor conductor of electric current. Electrodes B and C were assigned as boundary probes used to obtain the resulting potential, which was then used to obtain the transfer impedance. These simulations were performed to observe the impedance sensitivity distribution in a homogeneous volume and to verify that division by the tetrapole lengths allowed each data point to be scaled to the same level (Fig 6c). Moreover these simulations allowed for a performance comparison between the simulated stripe electrodes and the simulated as well as the experimental pseudo-stripe electrodes.

Further assessing research question (1), simulations were then carried out for eight models directly reproducing the gelatine phantom described previously, with blood vessel cylinder orientations of $\theta = -20°$, $-10°$, $0°$, $10°$, $20°$, $30°$, $60°$ and $90°$ with respect to the longitudinal axis of symmetry of the electrode array. The values of $\pm20°$ were chosen so as to verify that the model produced similar results to the experiments. For each θ simulations of SSVT sequences were carried out that led to estimates of the values of the $|Z_{ij}|$ matrix for each model, thus allowing for the selection of the electrode segments that were closer located to the blood vessel in each case. The $|Z_{ij}|$ matrix was then divided by the lengths of the related tetrapoles to remove the electrode spacing influence from the measurement. By applying a 10% threshold from the overall change in the impedance value, the desired segments satisfying research question (2) could be identified. The 10% threshold was selected empirically and it worked for all cases.

To assess research question (2) simulations were carried out for $\theta = -20°$ with the blood conductivity being varied from its original value (700.04 mS/m) that corresponded to the experiments up to twice that value (1400.08 mS/m), in increments of 10% . Moreover, uniquely in the simulations, an additional calculation was carried out for each conductivity

TABLE I: Expected segments vs identified segments

ϕ	Simulation		Experiment
	Expected	Identified	Identified
-20°	$AB = 1\ 2\ 3\ 4$ $CD = 5\ 6\ 7\ 8$	$AB = 1\ 2\ 3$ $CD = 6\ 7\ 8$	$AB = 1\ 2$ $CD = 6\ 7\ 8$
-10°	$AB = 2\ 3\ 4$ $CD = 5\ 6\ 7$	$AB = 2\ 3\ 4$ $CD = 5\ 6\ 7$	No Data
0°	$AB = 3\ 4\ 5\ 6$ $CD = 3\ 4\ 5\ 6$	$AB = 3\ 4\ 5\ 6$ $CD = 3\ 4\ 5\ 6$	No Data
10°	$AB = 5\ 6\ 7$ $CD = 2\ 3\ 4$	$AB = 5\ 6\ 7$ $CD = 2\ 3\ 4$	No Data
20°	$AB = 5\ 6\ 7\ 8$ $CD = 1\ 2\ 3\ 4$	$AB = 6\ 7\ 8$ $CD = 1\ 2\ 3$	$AB = 6\ 7\ 8$ $CD = 1\ 2\ 3$
30°	$AB = 1\ 2\ 3$ $CD = 6\ 7\ 8$	$AB = 1\ 2$ $CD = 7\ 8$	No Data
60°	$AB = 1\ 2$ $CD = 7\ 8$	$AB = 1\ 2$ $CD = 7\ 8$	No Data
90°	$AB = None$ $CD = None$	$AB = 1\ 2\ 7\ 8$ $CD = 1\ 2\ 7\ 8$	No Data

variation step of the blood vessel using stripe and pseudo-stripe electrodes, in order to establish whether they perform similarly.

III. RESULTS AND DISCUSSION

Both experimental and simulation results are presented and discussed for each research question.

A. Research Question (1)

1) Factoring in the weighting factor for different size tetrapole formations: Applying SSVT to the FEM saline-only volume resulted in a $|Z_{ij}|$ matrix Z_{S_SAL} which was then divided by the length Lt of each corresponding tetrapole, i.e. the outer edge-to-edge distance between the current injecting electrodes, to remove the electrode spacing influence from the measurement (Fig. 6). This resulted to normalised values that were within 3% of the average scaled value of the scaled Z_{S_SAL} dataset.

2) Scanning and localisation: Fig. 7(a) and (b) illustrate the data from the SSVT simulations for $\theta = -20°$ and $0°$ respectively. The scaling procedure was applied to all SSVT scans for both the experimental and the simulation results. The scaled results were then normalised to a $0\% - 100\%$ range and by applying a 10% threshold the desired segments were identified as shown by the examples in Fig. 7(c-f).

As the normalised figures indicate, the threshold can be used to identify the electrode pairs that correspond to the lowest impedance values. i.e. to the area over the blood vessel (top view). The ij combinations that are below the threshold are shown in Fig. 8 for $\theta = -20°$, together with the ij pairs geometrically located over the vessel labelled as expected segments. The outcome indicates a very close match of 85% with $12/14$ segments matching. For all cases of θ considered, Table 1 summarises the comparison between all of the AB_i-CD_j pairs found to exhibit the lowest $|Z_{ij}|$ values after scaling and normalising the results versus those located over the corresponding blood vessel. In most cases the results are very closely matched with the geometrically expected values.
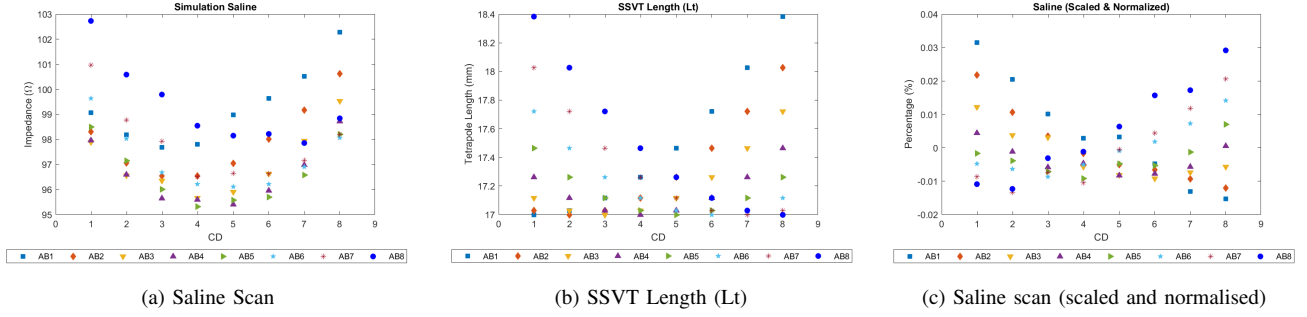
(a) Saline Scan

(b) SSVT Length (Lt)

(c) Saline scan (scaled and normalised)

Fig. 6: Scaling and Normalising data. a) saline scan data from simulation, b) Electrode tetra pole length, c) normalised and scaled data

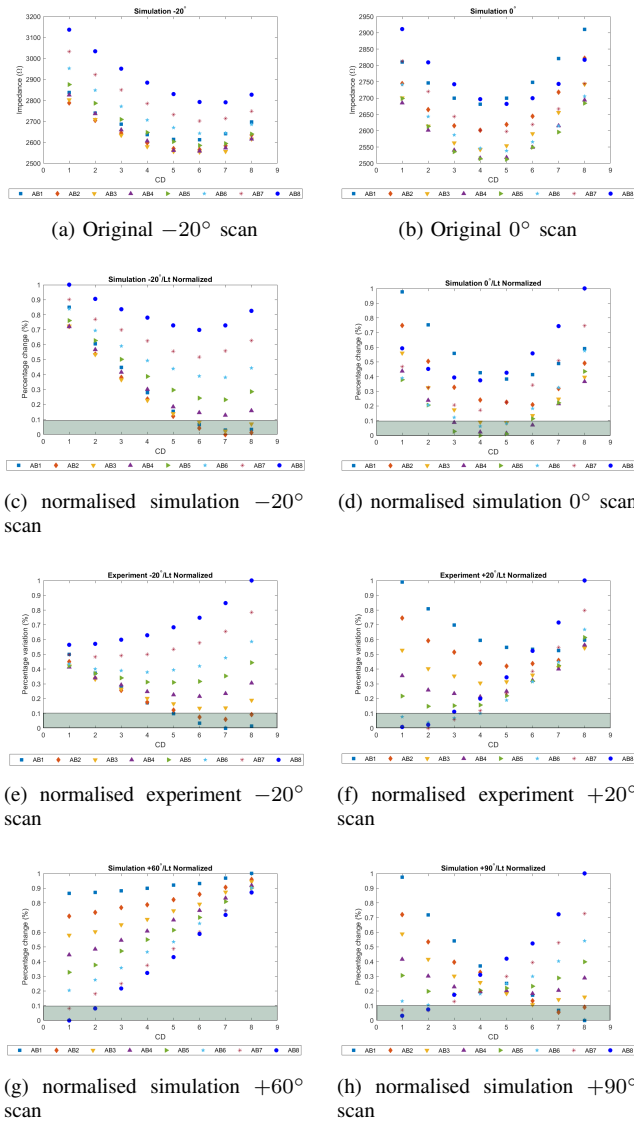(a) Original $-20°$ scan

(b) Original $0°$ scan

(c) normalised simulation $-20°$ scan

(d) normalised simulation $0°$ scan

(e) normalised experiment $-20°$ scan

(f) normalised experiment $+20°$ scan

(g) normalised simulation $+60°$ scan

(h) normalised simulation $+90°$ scan

Fig. 7: Blood vessel detection process. a) and b) show the original simulation scan data for $-20°$ and $20°$ orientations respectively. c-f) show the scaled and normalised simulation and experimental scan data for ($-20°$, $-10°$, $0°$, $10°$, $20°$, $60°$ and $90°$) orientation data, with a threshold of 10% of the maximum impedance
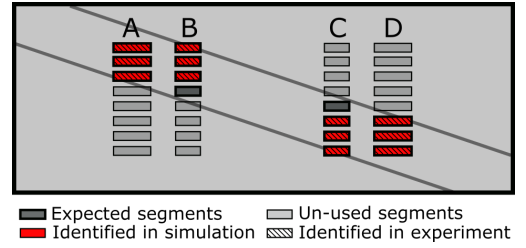

Fig. 8: Scan result plotted against electrode segments used to obtain results for detecting electrode segments overlapping the blood vessel

In non-controlled measurements, plotting the angle θ of each SSVT orientation ϕ vs the scaled normalised data provides an approximate value for the angle θ. This is shown in Fig. 9 for the $\theta = -20°$, $0°$, $20°$ cases where the lowest $|Z_{ij}|$ values exhibit minima at respective $\phi = -16.5°$, $-3.4°$, $0°$, $3.4°$, $16.5°$. These values are within 83% and thus approximately near the θ cases considered.

The scanning and localisation function of the system have been successfully demonstrated using the idealised model used here. It is worth mentioning that it does not take into consideration the anisotropic properties of muscle layer and the insulating properties of bone, or the influence of neighbouring vascular structures.

B. Research Question (2)

1) Pseudo- stripe vs full size stripe: The simulation results on saline solution with stripe and pseudo-stripe electrodes
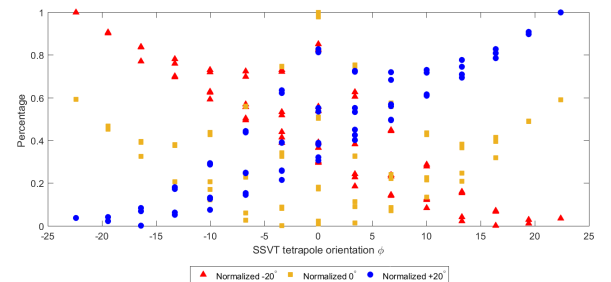

Fig. 9: SSVT orientation ϕ vs the scaled normalised data

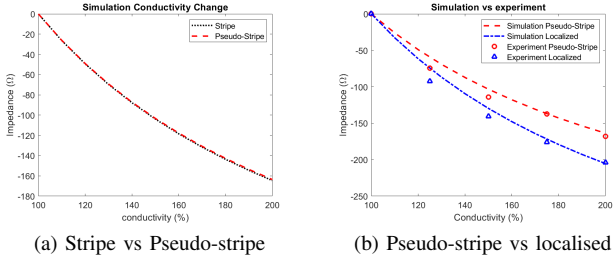(a) Stripe vs Pseudo-stripe   (b) Pseudo-stripe vs localised

Fig. 10: Impedance vs conductivity plot for simulation and experimental results, using different types of electrodes to measure impedance while changing conductivity of blood from 100% conductivity to 200% conductivity

demonstrated that the impedance for both types of electrodes was very similar: the simulated impedance for the stripe and for the pseudo-stripe electrodes for saline was 114.88 Ω and 115.41 Ω, respectively. The small difference of less than 1% between the two values leads to the conclusion that the pseudo-stripe electrodes emulate satisfactorily their equivalent stripe electrodes. Experimentally, the saline solution impedance was measured with an LCR meter and it was found to be 122 Ω. The difference of about 7 Ω with respect to the simulated value was attributed to the resistance introduced by the switching circuit.

It is expected that an increase in blood conductivity will result in a decrease of the total skin-fat-blood vessel impedance, and vice versa. Fig. 10a illustrates simulation results of the aforementioned blood conductivity variations worked out for stripe versus pseudo-stripe electrodes. The results are similar within 0.01% for all concentration steps, highlighting further the similarity in performance between full solid stripe electrodes and the grouping of segments covering a similar outline area.

2) Monitoring blood variations with localised vs. pseudo-stripe electrodes: Fig 10b illustrates the performance of localised electrodes comprising the selected ij pairs for θ = $-20°$ in the previous section, compared to pseudo-stripe electrodes in detecting such impedance changes, both with simulations and experimentally. The impedance measurement using the DRE localised electrodes overlapping the blood vessel is not the same as that monitored by the pseudo-stripe electrodes. The localised impedance measurements exhibit a larger decrease as a function of blood conductivity than when pseudo-stripe electrodes are used. A similar behaviour, albeit with a smaller relative difference is observed in the simulation results. The overall conclusion from these measurements is that, localised electrodes exhibit significantly higher sensitivity to blood variation. In fact absolute impedance change for each concentration step change is 25% higher for localised verses pseudo-stripe electrodes in simulations, while the corresponding experiment results exhibit a 22% $-$ 28% improvement. While this is a smaller variation than the one demonstrated in the theoretical lumped impedance model, the electrode length assumed in that model would have been significantly larger for the field lines to pass straight between the injecting electrodes.

Therefore it is commendable that, based on the achieved outcome, the localised electrodes exhibit higher sensitivity even when compared to relatively smaller stripe electrodes such as the ones examined here. This indicates that the performance improvement over significantly larger electrodes (eg: band electrodes) will be even more pronounced.

IV. CONCLUSION

A novel approach to using dynamically re-sizeable electrodes (DRE) in limb impedance plethysmography measurements is proposed in this paper. According to this approach, addressable and individually activated segmented electrodes are used rather than electrodes that cover large parts or even the whole limb. This approach has been investigated experimentally, in-vitro, using custom circuitry and gelatine phantoms. A corresponding FEM simulation model was also developed and used. A variable orientation and size single - segment scanning method (SSVT) was used in an attempt to identify electrode segments closest to the blood vessel in order to take more localised measurements.

From the results obtained in this paper it can be concluded that it is possible to utilise DRE in SSVT mode to approximately identify the transcutaneous location of the blood vessel being targeted. This information is then used to combine the electrode segments that are closer to the vessel so as to form effective localised electrodes covering the vessel only. Measurements taken using localised electrode segments identified through the SSVT scan indicate a significantly increased sensitivity to blood variations of up to 28% relative to larger electrodes. The DRE system could also potentially offer the advantages of reducing the need for accurate placement over a targeted vessel and of minimising the effects in the measurement of variations that relate to neighbouring vessels.

DRE was demonstrated to be advantageous in locating a vessel and in offering a better quality measurement than conventional methods, still there are some areas in designing and implementing such a system for diagnostics than require attention. In terms of electronics the interface circuits will be influenced by varying the effective electrode area which will change the contact impedance. Thus the injecting electronics output impedance should be designed accordingly. Other potential issues include influence by neighbouring vasculature and an increase in complexity in the circuitry relative to other impedimetric systems. In terms of application areas, the DRE will mainly be used for plethysmography to extract flow and volume information from arteries that are relatively solitary and in the extremities.

REFERENCES

[1] C. Corciova, M. Turnea, and A. Salceanu, "A measurement system for the blood flow in peripheral territory," *International Conference on E-Health and Bioengineering*, vol. 3, no. 4, pp. 1–4, 2011.

[2] J.-J. Wang, W.-C. Hu, T. Kao, C.-P. Liu, and S.-K. Lin, "Development of forearm impedance plethysmography for the minimally invasive monitoring of cardiac pumping function," *Journal of Biomedical Science and Engineering*, vol. 04, no. 02, pp. 122–129, 2011.

[3] B. D. Nenova, I. T. Iliev, and A. Photoplethysmography, "Non-Invasive Methods of Peripheral Pulse Detection : Advantages and Disadvantages," *ANNUAL JOURNAL OF ELECTRONICS*, pp. 57–60, 2009.

[4] F. A. Anderson, "Impedance plethysmography in the diagnosis of arterial and venous disease," *Annals of Biomedical Engineering*, vol. 12, no. 1, pp. 79–102, 1 1984.

[5] S. Grimnes and . G. Martinsen, *Bioimpedance and Bioelectricity Basics*. Elsevier, 2015.

[6] R. W. Gotshall and W. R. Sexson, "Comparison of band and spot electrodes for the measurement of stroke volume by the bioelectric impedance technique," *Critical Care Medicine*, vol. 22, no. 3, pp. 420–425, 1994.

[7] S. H. Liu, D. C. Cheng, and C. H. Su, "A Cuffless Blood Pressure Measurement Based on the Impedance Plethysmography Technique," *Sensors (Basel, Switzerland)*, vol. 17, no. 5, pp. 1–13, 2017.

[8] T. H. Huynh, R. Jafari, and W. Y. Chung, "Noninvasive Cuffless Blood Pressure Estimation Using Pulse Transit Time and Impedance Plethysmography," *IEEE Transactions on Biomedical Engineering*, vol. PP, no. c, p. 1, 2018.

[9] E. Mašanauskiene, S. Sadauskas, A. Naudžiunas, A. Unikauskas, and E. Stankevičius, "Impedance plethysmography as an alternative method for the diagnosis of peripheral arterial disease," *Medicina (Lithuania)*, vol. 50, no. 6, pp. 334–339, 2014.

[10] I. C. Henry, D. P. Bernstein, and M. J. Banet, "Stroke volume obtained from the brachial artery using transbrachial electrical bioimpedance velocimetry," *Proceedings of the Annual International Conference of the IEEE Engineering in Medicine and Biology Society, EMBS*, no. 3, pp. 142–145, 2012.

[11] M. Qu, Y. Zhang, J. G. Webster, and W. J. Tompkins, "Motion Artifact from Spot and Band Electrodes During Impedance Cardiography," *IEEE Transactions on Biomedical Engineering*, vol. BME-33, no. 11, pp. 1029–1036, 1986.

[12] A. Ikarashi, M. Nogawa, T. Yamakoshi, S. Tanaka, and K. I. Yamakoshi, "An optimal spot-electrodes array for electrical impedance cardiography through determination of impedance mapping of a regional area along the medial line on the thorax," *Annual International Conference of the IEEE Engineering in Medicine and Biology - Proceedings*, pp. 3202–3205, 2006.

[13] Y. Tomiyama, K. Yoshinaga, S. Fujii, N. Ochi, M. Inoue, M. Nishida, K. Aziki, T. Horie, C. Katoh, and N. Tamaki, "Accurate quantitative measurements of brachial artery cross-sectional vascular area and vascular volume elastic modulus using automated oscillometric measurements: Comparison with brachial artery ultrasound," *Hypertension Research*, vol. 38, no. 7, pp. 478–484, 2015. [Online]. Available: http://dx.doi.org/10.1038/hr.2015.6

[14] C. Gabriel, "Compilation of the Dielectric Properties of Body Tissues at RF and Microwave Frequencies," *Tech. Report, Dep. Physics, King's Coll. London*, vol. Report No., no. June, p. 21, 1996.

[15] A. Seo, M. Rys, and S. Konz, "Measuring lower leg swelling: Optimum frequency for impedance method," *Medical and Biological Engineering and Computing*, vol. 39, no. 2, pp. 185–189, 2001.

[16] F.-J. Pettersen and J. O. Høgetveit, "From 3D tissue data to impedance using Simpleware ScanFE+IP and COMSOL Multiphysics a tutorial," *Journal of Electrical Bioimpedance*, vol. 2, no. 1, pp. 13–32, 2011.

[17] A. T. Mobashsher and A. M. Abbosh, "Artificial human phantoms: Human proxy in testing microwave apparatuses that have electromagnetic interaction with the human body," *IEEE Microwave Magazine*, vol. 16, no. 6, pp. 42–62, 2015.

[18] D. Bennett, "NaCl doping and the conductivity of agar phantoms," *Materials Science and Engineering C*, vol. 31, no. 2, pp. 494–498, 2011.

[19] T. J. Kao, G. J. Saulnier, D. Isaacson, T. L. Szabo, and J. C. Newell, "A versatile high-permittivity phantom for EIT," *IEEE Transactions on Biomedical Engineering*, vol. 55, no. 11, pp. 2601–2607, 2008.

[20] C. Gabriel, S. Gabriel, and E. Corthout, "The dielectric properties of biological tissues: {I. Literature} survey," *Physics in medicine and biology*, vol. 41, no. 11, p. 2231, 1996.

[21] ——, "The dielectric properties of biological tissues: III. Parametric models for the dielectric spectrum of tissues," *Physics in Medicine and Biology*, vol. 41, no. 11, pp. 2271–2294, 2000. [Online]. Available: http://iopscience.iop.org/article/10.1088/0031-9155/41/11/003/pdf

[22] P. Hua, E. J. Woo, J. G. Webster, and W. J. Tompkins, "Using compound electrodes in electrical impedance tomography." *IEEE transactions on bio-medical engineering*, vol. 40, no. 1, pp. 29–34, 1993.

[23] J.-j. Huang, Y.-m. Huang, and A. R. See, "Velocity Using Bio-impedance Plethysmography and Regression Analysis," *ECTI TRANSACTIONS ON COMPUTER AND INFORMATION TECHNOLOGY*, vol. 11, no. 1, pp. 63–70, 20117.

[24] F. Lu, C. Wang, R. Zhao, L. Du, Z. Fang, X. Guo, and Z. Zhao, "Review of stratum corneum impedance measurement in non-invasive penetration application," *Biosensors*, vol. 8, no. 2, 2018.

[25] V. De Santis, V. Martynyuk, A. Lampasi, M. Fedula, and M. D. Ortigueira, "Fractional-order circuit models of the human body impedance for compliance tests against contact currents," *AEU - International Journal of Electronics and Communications*, vol. 78, pp. 238–244, 2017.

[26] R. Ivanic, I. Novotny, V. Rehacek, V. Tvarozek, and M. Weis, "Thin film non-symmetric microelectrode array for impedance monitoring of human skin," *Thin Solid Films*, vol. 433, no. 1-2 SPEC., pp. 332–336, 2003.

[27] J. Petrofsky, E. Schwab, M. Cúneo, J. George, J. Kim, A. Almalty, D. Lawson, E. Johnson, and W. Remigo, "Current distribution under electrodes in relation to stimulation current and skin blood flow: Are modern electrodes really providing the current distribution during stimulation we believe they are?" *Journal of Medical Engineering and Technology*, vol. 30, no. 6, pp. 368–381, 2006.

[28] A. Lozano, J. Rosell, and R. Pallás-Areny, "Two-frequency impedance plethysmograph: real and imaginary parts," *Medical & Biological Engineering & Computing*, vol. 28, no. 1, pp. 38–42, 1 1990.

[29] E. D. Smith, F. Szidarovszky, W. J. Karnavas, and A. T. Bahill, "Sensitivity Analysis, a Powerful System Validation Technique," *The Open Cybernetics & Systemics Journal*, vol. 2, no. 1, pp. 39–56, 2 2007.

[30] Keysight, "Keysight E4980A/AL Precision LCR Meter," 2017.